

# In-situ Polymerized Single Lithium-ion Conducting Binder as an Integrated Strategy for High Voltage LNMO Electrodes

Jorge Olmedo-González,<sup>[a]</sup> Gregorio Guzmán-González,<sup>[b]</sup> Arturo Manzo-Robledo,<sup>[a]</sup> Daniel Ramírez-Rosales,<sup>[c]</sup> Stephany N. Arellano-Ahumada,<sup>[c]</sup> Marco A. Vera-Ramírez,<sup>[b]</sup> Ignacio González,<sup>[b]</sup> Rosa de Guadalupe González-Huerta,<sup>[a]</sup> and Guadalupe Ramos-Sánchez<sup>\*[d]</sup>

High voltage spinel  $\text{LiNi}_{0.5}\text{Mn}_{1.5}\text{O}_4$  (LNMO) is a promising material for next generation lithium-ion batteries. However, its reactivity near 5 V possess stability and cycling challenges. In this study, a novel integrated approach is employed using a single lithium-ion conducting polymer binder (SLICPB) to prevent interactions with reactive anions and create a protective layer against electrolyte decomposition. The proposed SLICPB in-situ polymerization in the LNMO electrodes simplifies the preparation process, reducing costs. SLICPB properties effectively decrease polarization by concentration. For instance,

at a discharge capacity of  $68 \text{ mAh g}^{-1}$ , the voltage hysteresis difference is 0.31 V, enabling higher capacity at 1 C (a 38% increase) compared to traditional binder electrodes. Notably, this integrated strategy completely replaces the traditional binder without any need for additives, thus avoiding any extra weight in the electrode preparation. Furthermore, SLICPB properties successfully decrease reactivity and diminish the leaching of  $\text{Mn}^{2+}$ , as evaluated through differential electrochemical mass spectrometry and electron paramagnetic resonance, respectively.

## Introduction

The development of next-generation lithium-ion batteries (LIBs) focus on achieving higher energy density and improved stability. However, aside from electrochemical properties, factors such as the cost of cathode preparation and its environmental impact also hold significance.<sup>[1,2]</sup> The cathode material,  $\text{LiNi}_{0.5}\text{Mn}_{1.5}\text{O}_4$  (LNMO), has demonstrated significant potential for enhancing energy density, boasting an operating voltage of 4.7 V and a theoretical capacity of  $147 \text{ mAh g}^{-1}$ . Its redox processes  $\text{Ni}^{2+} \rightarrow \text{Ni}^{4+}$ , and the stabilizing effect of manganese provide the conditions for a superb cathode material.<sup>[3,4]</sup> Nonetheless, the

operating voltage above 4.2 V is far beyond the stability window for most of the electrolytes for LIBs. This leads to the degradation of electrolyte solvents into gases, primarily  $\text{CO}_2$ , which occurs in LNMO electrodes during oxidation between 4.5 and 5 V.<sup>[5,6]</sup> While some solid polymers have been proposed as alternative electrolytes with improved stability, the low intrinsic conductivity and limited interfacial compatibility have hindered significant gains in energy density.<sup>[7,8]</sup> LNMO also exhibits dissolution of the  $\text{Mn}^{2+}$  in the electrolyte, stemming from the disproportionation reaction that poses challenges to structural stability and cycle life.<sup>[9–12]</sup> Conversely, the reactions involving  $\text{PF}_6^-$  anions at high voltages contribute significantly to degradation, as continuous reactivity leads to the formation of various fluorinated compounds that further worsen degradation.<sup>[13]</sup> To address these problems, certain additives, particularly those based on borate anions, have been successfully incorporated to decrease the surface reactivity of  $\text{PF}_6^-$ . However, the approach of adding additives suffers intrinsic drawbacks. Firstly, the development of protective layers occurs during cycling, resulting in different types of compounds (and rates of formation) based on the operating conditions. Secondly, the process is gradual and typically requires several formation cycles.<sup>[14–16]</sup>

Single lithium-ion conducting polymer electrolytes (SLICPEs) belong to a special class of polymers with transport numbers approaching unity. They are typically more stable than their liquid counterparts.<sup>[17,18]</sup> SLICPEs incorporating  $\text{sp}^3$  boron atoms and polyethylene glycol bridges have emerged as promising functional materials. They offer the flexibility to modify polymer coordination, manipulate pendant groups, and enhance ion mobility.<sup>[19–22]</sup> In this study, we capitalize on these attributes by proposing them not as an electrolyte but as a binder, referred to

[a] J. Olmedo-González, Dr. A. Manzo-Robledo, Dr. R. de Guadalupe González-Huerta

*Instituto Politécnico Nacional  
Escuela Superior de Ingeniería Química e Industrias Extractivas  
UPALM, 07738 Mexico City (México)*

[b] Dr. G. Guzmán-González, M. A. Vera-Ramírez, Dr. I. González  
*Departamento de Química  
Universidad Autónoma Metropolitana-Iztapalapa  
Av. San Rafael Atlixco 186, 09340 Mexico City (México)*

[c] Dr. D. Ramírez-Rosales, S. N. Arellano-Ahumada  
*Instituto Politécnico Nacional  
Escuela Superior de Física y Matemáticas  
UPALM, 07738 Mexico City (México)*

[d] Dr. G. Ramos-Sánchez  
*Departamento de Ingeniería de Procesos e Hidráulica  
Universidad Autónoma Metropolitana-Iztapalapa  
Av. San Rafael Atlixco 186, 09340 Mexico City (México)  
E-mail: gramos@xanum.uam.mx*

Supporting information for this article is available on the WWW under  
<https://doi.org/10.1002/batt.202300383>

as a single lithium-ion conducting polymer binder (SLICPB).<sup>[23,24]</sup> In this approach, the polymer is employed to coat the active material particles, forming an engineered cathode-electrolyte interface (CEI) with potential protective properties.<sup>[25,26]</sup> Notably, the total replacement of the conventional binder with SLICPB introduces no additional weight to the electrode, a common issue when incorporating inorganic coatings or additives to the active material or electrolyte. Moreover, SLICPBs offer the advantage of facilitating the electrode fabrication process in a single step, avoiding the requirement for traditional solvent mixing, application, and drying on the current collector procedures.<sup>[27]</sup> This approach diminishes the energy demand, as the volatile solvent can be easily removed during drying. Several studies have indicated that the most energy-intensive stages in LIBs manufacturing are solvent recovery and formation/aging, accounting for 47% and 30% of the energy consumption, respectively. Consequently, these stages also contribute significantly to the overall manufacturing cost, comprising 15% and 32% of the total expenses.<sup>[28,29]</sup> By employing in-situ polymerization in the presence of the active material, we achieve the direct deposition of the material onto the current collector using methanol as a volatile solvent; thus, carcinogenic N-methyl-2-pyrrolidone is substituted, increasing the sustainability of the fabrication process. Additionally, the utilization of SLICPBs significantly decreases the number of cycles required to form a stable cathode interface, further enhancing the energy efficiency of fabrication.<sup>[30]</sup>

This novel study evaluates the impact of SLICPBs on the durability of LNMO electrodes, we conducted comprehensive electrochemical characterization and employed advanced techniques to demonstrate the benefits of a boron based SLICPB such as differential electrochemical mass spectrometry (DEMS) and electron paramagnetic resonance (EPR). Solid-state nuclear magnetic resonance (ss-NMR) spectroscopy and Fourier-transform infrared spectroscopy (FTIR) were also employed to study the interaction between SLICPB and LNMO material. Through the integration of these methods, we can effectively harness the advantages of combining new materials and electrode preparation methods to enhance the global electrochemical performance of cells assembled with composite LNMO electrodes.

## Results and Discussion

To prepare the electrodes, freshly synthesized  $\text{LiB}(\text{OCH}_3)_4$  (LTMB) was used as precursor for the in situ polymerization with Polyethylene glycol (PEG-400) to obtain a boron-based SLICPB known as BEG when combined with LNMO powder.<sup>[31–33]</sup> It should be noted that although the properties of this polymer as electrolyte have been reported, in this study, it is used as binder, completely replacing PVDF binder. The formation of a homogeneous LTMB compound, composed only of tetrahedral moieties, was confirmed by  $^7\text{Li}$  and  $^{11}\text{B}$  solid ss-NMR (Figure 1a (trace i) and 1b (trace i)), respectively. BEG was prepared using varying amounts of SLICPB and LNMO powder, *i.e.*, BEG<sub>97</sub> (SLICPB 97 wt%-LNMO 3 wt%) to study their interactions. After in-situ polymerization, the  $^{11}\text{B}$  NMR spectrum exhibits a peak shoulder,

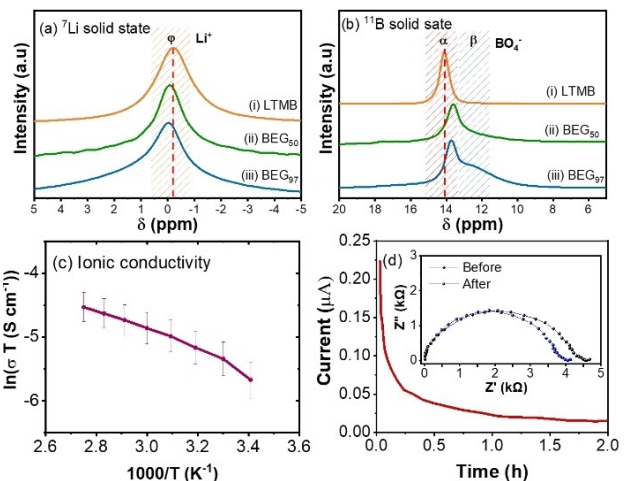


**Figure 1.** a)  $^7\text{Li}$  and b)  $^{11}\text{B}$  NMR/MAS at 8 kHz spectra of the synthesized boron-based SLICPB, (i)  $\text{LiB}(\text{OCH}_3)_4$ , (ii) BEG<sub>50</sub>, (iii) BEG<sub>97</sub>. The chemical groups associated with the signals are indicated as  $\varphi$  for  $\text{Li}^+$ ,  $\alpha$ , and  $\beta$  for two chemical environments of  $\text{BO}_4^-$ , c) Arrhenius plot of ionic conductivity of the synthesized boron-based SLICPB (BEG<sub>100</sub>), d) lithium transfer number ( $t_{\text{Li}^+}$ ) evaluation: typical current transient obtained at a polarization of 10 mV for  $\text{Li}^0/\text{BEG}_{100}/\text{Li}^0$  cells at 25 °C (inset: Nyquist plot for BEG, both before and after polarization).

whose displacement towards high field (protection of the borate group) indicates an interaction between the borates and the surface of the active material, resulting in distinct types of borate groups (Figure 1b, traces ii and iii). One of these borate groups displayed complete tetrahedral geometry, while the other exhibits slight modifications. The  $^7\text{Li}$  NMR spectra of BEG<sub>50</sub> and BEG<sub>97</sub> samples reveal a single peak close to 0 ppm. The slight shift of this signal towards low field (unprotection of the lithium atoms) corroborates the decoupling of the lithium ions as a consequence of their co-propagation with the surface of the LNMO particles by interaction with the borate groups. However, upon in situ polymerization, the presence of two peaks became evident, with one attributed to the SLICPB and the other associated with lithium in LNMO (Figure S1).<sup>[34]</sup>

To assess the impact of SLICPB on LNMO, FTIR was also performed using different proportions of SLICPE and LNMO (Figure S2). The FTIR spectra of LTMB and BEG<sub>100</sub> exhibited characteristic  $\text{BO}_4^-$  bands near  $990 \text{ cm}^{-1}$ , while missing bands at  $1300 \text{ cm}^{-1}$  confirm the absence of  $\text{BO}_3$  in the materials. The characteristic  $\text{BO}_4^-$  band exhibits a slight shift towards higher wavenumbers as the amount of LNMO increased, confirming the presence of two distinct chemical environments of  $\text{BO}_4^-$ , consistent with the findings from ss-NMR analysis. Furthermore, the ionic conductivity of SLICPB is similar and in some cases superior to that of other polymer electrolytes (table S1),<sup>[35–38]</sup> with the advantage to having the transport number close to unity at all temperatures, confirming its single-ion conducting capability (Figure 1c and d).<sup>[39]</sup>

Upon electrode preparation and confirmation of the SLICPB structure on the particles, cyclic voltammetry was employed as the primary tool to investigate the changes occurring at high potentials. By subjecting the system to prolonged operation at higher potentials, cyclic voltammetry ( $v=0.1 \text{ mVs}^{-1}$ ) allows for

the examination of potential-induced durability effects. Since all the electrochemical processes occur at potentials above 4.8 V, which exceeds the typical stability window of conventional electrolytes, high reactivity is expected. A comparison was made between electrodes comprising the traditional polyvinylidene fluoride (PVDF) binder, referred to as active material fluorine binder (AMFB), and SLICPB referred to as active material boron binder (AMBB) electrodes (Figure 2) and they were prepared with conductive carbon black (CCB). In both samples, the main redox processes take place at potentials higher than 4.6 V, primarily associated with transformations from  $\text{Ni}^{2+}$  to  $\text{Ni}^{4+}$  (Figure 2ii), while those related to the Mn redox process are nearly negligible (Figure 2i). Initially, AMBB exhibits a higher peak-to-peak separation, probably attributed to the inherent resistance of the binder. However, during cycling, the peak current decreases while the peak potentials for both oxidation and reduction remain unchanged. In contrast, AMFB exhibits a decrease in peak current without a significant change in peak potentials, indicating a significant degradation problem (Figure 2ii). Another noteworthy finding from CV is the current density at potentials close to 5 V. Initially, At this potential in the first cycle, AMFB shows a current density similar to that of AMBB, nonetheless the current density for AMFB continues rising as cycling increases, indicating high reactivity most probably due to the oxidation of species either in the electrolyte or in the interphase. Conversely, for AMBB, not only the current is lower for the first cycle, but it further decreases as cycling progresses until the end of the tests (Figure 2 iii).

Galvanostatic measurements are widely used for battery characterization. In the case of both binders, the initial capacity at 0.1 C is similar (Figure 3a). However, a closer examination reveals two significant differences. Firstly, the slope of the curve at the end of oxidation is much higher for AMBB compared to AMFB, probably indicating lower reactivity at higher potentials and suggesting the protective effect of SLICPB, similar to that

obtained through CV. Secondly, during discharge, there is a slight yet noticeable decrease in the discharge potential towards the end, a behavior traditionally associated with polarization by concentration resulting from a depletion of species near the electrodes, table S2 provide values for discharge potentials using both binders where the advantages of AMBB are evident.<sup>[40]</sup> The constant presence of mobile  $\text{Li}^+$  in SLICPB helps mitigate polarization by concentration, providing an additional advantage; in this regard, it is important to highlight that although the beneficial impact of several binders in protective capability has been reported, no material has been reported to diminish polarization by concentration due to the SLICPBs.<sup>[41-44]</sup> At higher C-rates, the disparities between the binders are exacerbated, with a greater difference in capacity between the samples, being higher for AMBB. Furthermore, the slope of the charge curve at high potential remains significantly steeper for AMBB compared to AMFB, and the plateau separation increases as the C-rate rises (Figure 3b-d). Two main differences are noteworthy; the occurrence of polarization by anionic concentration during discharge, which is mitigated by SLICPB providing a continuous supply of lithium ions, and the oxidation behavior at potentials close to 5 V, suggesting lower interfacial reactivity.<sup>[45]</sup> dQ/dV curves prepared for these potentials clearly demonstrate the advantages offered by SLICPB (Figure 3e-h). It is worth noting a slightly higher oxidation current in AMFB near 5 V, possibly attributed to electrolyte reactivity at high potentials (for a closer inspection check Figure S3); moreover, during discharge, AMBB presents well-defined peaks, associated with well-defined plateaus, while for AMFB the peaky behavior is lost even at 0.5 C. The C-rate capability behavior over 100 cycles (Figure 3i) indicates that AMBB exhibits improved capacity retention compared to AMFB, showing a difference of  $28 \text{ mAh g}^{-1}$  at 1 C and high capacity retention when returning to slow rates.

Further experiments conducted for 500 cycles at 1 C provide additional confirmation of the advantages of SLICPB (Figure 4).

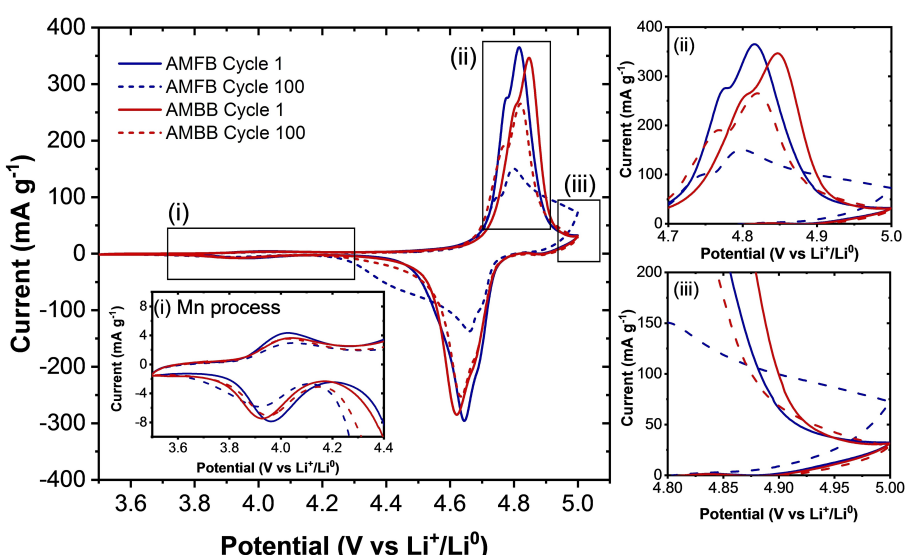


**Figure 2.** Cyclic voltammograms of AMFB and AMBB electrodes 1<sup>st</sup> and 100<sup>th</sup> cycles ( $v=0.1 \text{ mVs}^{-1}$ ) obtained for  $\text{Li}^0/1 \text{ M LiPF}_6 \text{ EC:DMC:EMC } 1:1:1$  / (LNMO-CCB-binder: 80-10-10 wt%) at room temperature. i) amplified region of 3.4–4.4 V for  $\text{Mn}^{3+}/^{4+}$  process, ii) amplified region of 4.7–5.0 V for  $\text{Ni}^{2+}/^{4+}$  process and iii) amplified region of 4.8–5.0 V centered in the reactivity during the oxidation at high potentials.

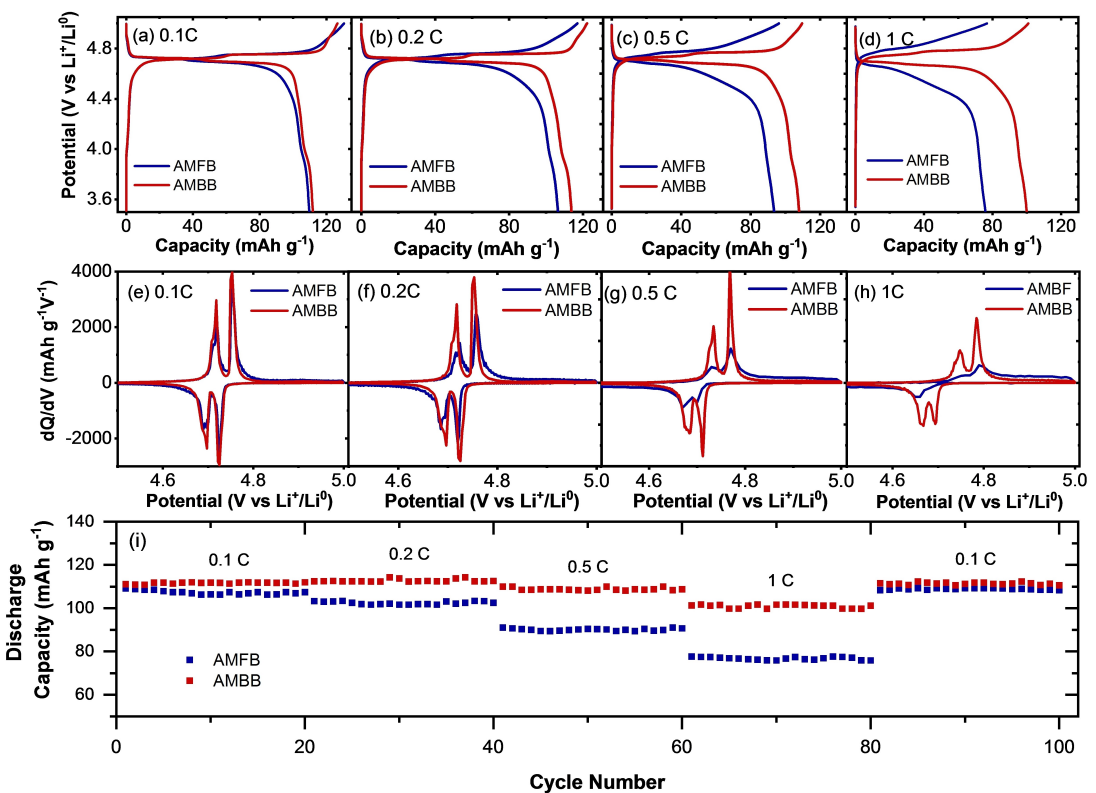


**Figure 3.** Charge/discharge profiles of AMFB and AMBB electrodes obtained for Li<sup>0</sup>/1 M LiPF<sub>6</sub> EC:DMC:EMC 1:1:1/ (LNMO-CCB-binder: 80–10–10 wt %) at room temperature. a) 0.1 C, b) 0.2 C, c) 0.5 C, d) 1 C, dQ/dV profiles of AMFB and AMBB electrodes e) 0.1 C, f) 0.2 C, g) 0.5 C, h) 1 C, i) C-rate capability of AMFB and AMBB electrodes.

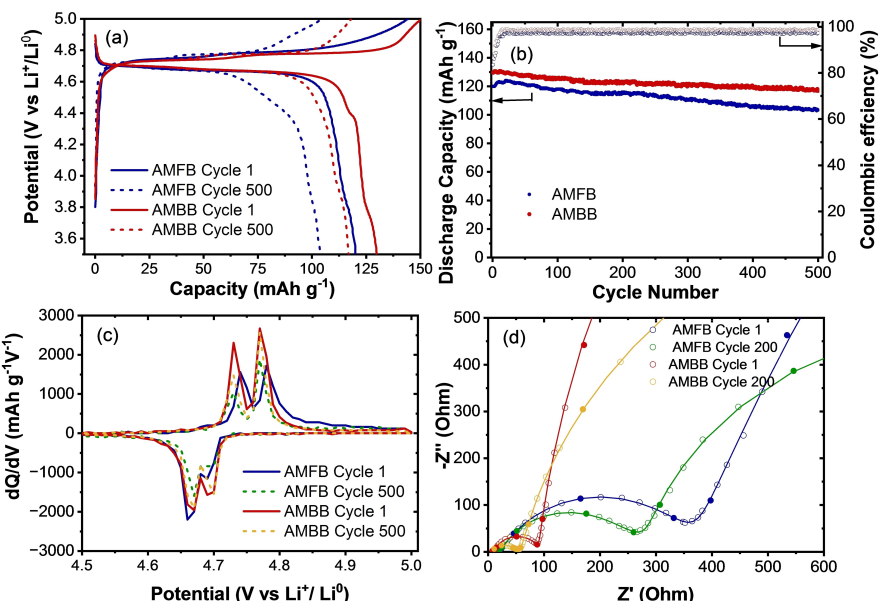


**Figure 4.** AMFB and AMBB electrodes in an Li<sup>0</sup>/1 M LiPF<sub>6</sub> EC:DMC:EMC 1:1:1/ (LNMO-CCB-binder: 80–10–10 wt %) cells at room temperature. a) Charge/discharge voltage profiles at 1 C, 1<sup>st</sup> and 500<sup>th</sup> cycles. b) Capacity retention plots for the cells cycled at 1 C for 500 cycles. c) dQ/dV profiles 1 C, 1<sup>st</sup> and 500<sup>th</sup> cycles. d) Nyquist plots obtained at 3.8 V in the 1<sup>st</sup> and 200<sup>th</sup> cycles.

One of the key benefits offered by this binder is the diminished polarization by concentration. Since most of the literature focuses only on capacity, it is crucial to consider the potential as well. AMFB leads to a decrease in lithium concentration near the

surface as discharge progresses. In contrast, the inherent nature of SLICPB provides a continuous supply of lithium ions near the surface, resulting in a difference of at least 70 mAh g<sup>-1</sup> and a plateau that remains flat during the discharge process. Other

approaches have reported capacity decay of around 13% after 300 cycles in comparison we obtain 6% decay at the same number of cycles and 7–6% for 500 cycles (Figure 4b).<sup>[41,44,46]</sup> Likewise, dQ/dV plots (Figure 4c) confirm a clear pattern of voltage plateau degradation becomes evident after 500 cycles. AMFB exhibits slightly higher reactivity during oxidation at high potentials compared to AMBB and that the plateau-like behavior is lost during cycling.

The Nyquist plots for the impedance spectra obtained for the cells assembled with the AMFB and AMBB electrodes (Figure 4d) exhibit notable differences, while still retaining the characteristic features of a semicircle at medium frequencies and a straight line at lower frequencies. However, the size of the semicircle is notably smaller for AMBB electrodes, indicating lower impedance values associated with the unique nature of the SLICPB binder. After 200 cycles, both electrodes show a decrease in impedance for the various processes, suggesting improved performance as a result of cycling.<sup>[47,48]</sup> Further quantitative analysis using equivalent circuits<sup>[49,50]</sup> (Figure S4 and Table S3, nomenclature and definitions can be found in Supporting Information as well) confirms that  $R_{SEI}$  is lower for AMBB than AMFB electrodes, while  $C_{SEI}$  exhibits the opposite trend, potentially attributed to the single lithium capability and electrode preparation. Additionally, AMBB demonstrates significantly lower values of  $R_{ct}$  and  $C_{dl}$  values than AMFB, indicating enhanced charge transfer kinetics and potentially higher power performance in the charge transfer and electric double-layer region.<sup>[51]</sup>

Gases and volatile species generated during electrochemical experiments, particularly at high potentials, have played a crucial role in evaluating the protective effect of different coatings or binders.<sup>[52]</sup> To enhance species production, the electrodes are polarized at 5.0 V after full charging and then maintained the voltage at 4.8 V while analyzing the resulting faradic current and species using mass spectrometry. The DEMS analysis (Figure S5) confirms the observations made in dQ/dV and CV plots. The main focus was on  $m/z=44$  (Figure 5a),<sup>[53]</sup> although other species were also analyzed, such as  $m/z=2$ ,  $m/z=28$ , and  $m/z=32$  (Figure S6). In the case of AMFB, the production of  $\text{CO}_2$  is observed after 5 minutes, reaching a maximum and slowly starting to decrease. There is a significant difference in AMBB, where the signal is negligible. These variations observed in AMFB could be attributed to changes in the cathode surface.<sup>[54]</sup> It has been noted that the presence of  $\text{Li}_2\text{CO}_3$  during the formation of the CEI can lead to the generation of  $\text{CO}_2$  and  $\text{O}_2$ . When these gases react with the solvents of the electrolyte (EC, DMC, and EMC),  $\text{CO}_2$  and CO are produced during battery oxidation.<sup>[55–57]</sup> So far, these results effectively demonstrate that AMBB electrodes, produced using the in-situ polymerization method are indeed capable of decreasing surface reactivity at higher potentials, successfully improving cyclability and stability.

In addition, the glass fiber separator was removed after 500 cycles and subjected to analysis using EPR.<sup>[58]</sup> A few EPR studies have confirmed  $\text{Mn}^{2+}$  in LNMO cathodes promoted by the generation of hydrofluoric acid (HF).<sup>[59]</sup> The EPR response indicates the presence of  $\text{Mn}^{2+}$  ions, as expected from manganese disproportionation reactions and eventual leaching into the electrolyte. These findings corroborate the results

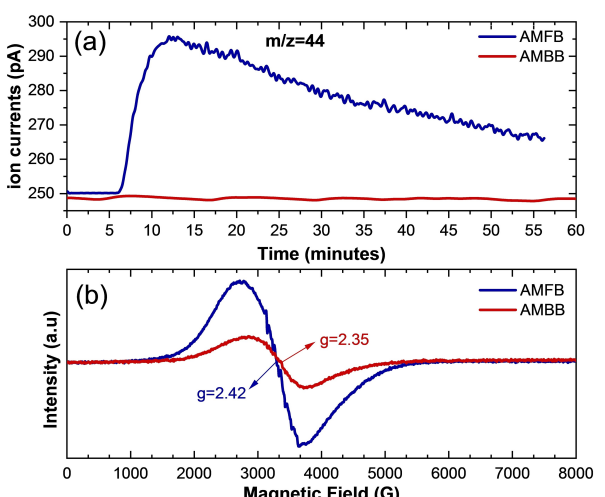


**Figure 5.** AMFB and AMBB electrodes in an  $\text{Li}^0/1 \text{ M LiPF}_6$  EC:DMC:EMC 1:1:1/LNMO-CCB-binder: 80-10-10 wt % cells at room temperature. a)  $m/z=44$  mass spectrometric signals during the charge through a chronoamperometric evaluation at 5 V in DEMS analysis, b) EPR spectra for  $\text{Mn}^{2+}$  of AMFB and AMBB separator samples after 200 cycles, exhibiting different line widths and intensities.

obtained from electrochemical impedance spectroscopy. It is evident that the SLICPB is not able to completely prevent the reactions within the electrode, as  $\text{Mn}^{2+}$  is still formed. However, due to single-lithium conducting nature, it likely mitigates the presence of  $\text{PF}_5^-$  anions and its decomposition products (among them HF), which has a significant impact on the stability of the material and the leaching of  $\text{Mn}^{2+}$  ions (Figure 5b). The EPR spectra (Figure S7) obtained from the cathode reveal (not the electrolyte) a g value below and around 2, indicating the presence of both  $\text{Mn}^{3+}$  (LNMO spinel structure) and  $\text{Mn}^{2+}$ , respectively. This provides further evidence for the cathode disproportionation effect and supports the discussion regarding the leaching of  $\text{Mn}^{2+}$  into the electrolyte.

## Conclusions

The use of in-situ polymerization for preparation and complete replacement of PVDF binder with a novel boron-based SLICPB in LNMO high voltage cathode results in significantly enhanced cyclability, decrease polarization by concentration, improved capacity, and overall enhanced performance. The SLICPB was found to be beneficial in enhancing ionic conduction and preserving electrode utilization, resulting in less deterioration. Excellent electrochemical performance was observed for AMBB, exhibiting a capacity retention of nearly 90% after 500 cycles at a 1 C rate.

Further diagnostic studies utilizing DEMS and EPR techniques reveal that the superior stability of AMBB not only decreases  $\text{Mn}^{2+}$  leaching but also maintains the stability of the electrolyte during battery cycling. Conversely, AMFB experienced significant structural and electrolyte changes, leading to lower ionic conductivity compared to AMBB. These findings emphasize the substantial influence of the binder on enhancing the cycle life of

LNMO lithium-ion batteries. Although the synthesis method and overall the electrochemical properties are enhanced, due to the natural crosslinking of the boron based binder the electrodes are less flexible. In order to improve them, mechanical tests such as tensile test, peeling strength, and swelling test must be conducted to ensure the compatibility of the binder with the electrolyte and its adhesion to the substrate, these results will be published elsewhere.<sup>[60]</sup> This straightforward and cost-effective approach has the potential to ediminish battery preparation costs, making it a promising candidate for significant advancements in the battery industry. Implementing these technologies at an industrial scale could be one of the most significant breakthroughs in the field.

## Experimental Section

### SLICPB preparation

The method employed to obtain the boron-based SLICPB consists of two stages. In Stage 1, the synthesis of lithium tetramethoxy borate LiB(OCH<sub>3</sub>)<sub>4</sub> (LTMB) involves two distinct reactions. The first reaction focuses on obtaining lithium methanolate (CH<sub>3</sub>OLi), while the second reaction involves the production of LTMB using trimethyl borate B(OCH<sub>3</sub>)<sub>3</sub>. This synthesis route has been proven to be highly effective in the formation of tetracoordinate boron compounds. Moving on to Stage 2, the synthesis of SLICPB involves an *in situ* polycondensation reaction with the addition of Polyethylene glycol (PEG 400), which becomes linked by borate units.<sup>[31]</sup> One notable advantage of this synthesis method is that the polymerization process is easily triggered by simple heating. Furthermore, when this synthesis is carried out in the presence of the electrode components, the electrode is directly formed on the current collector or aluminum substrate, as depicted in Figure S1.

### Electrochemical characterization

AMFB electrodes were prepared by mixing LNMO (MTI), conductive carbon black (Super P, MTI), and polyvinylidene fluoride (PVDF, Sigma-Aldrich) at a mass ratio of 80/10/10 with NMP (N-methyl pyrrolidone, Sigma-Aldrich) for 6 hours. The ink was coated onto aluminum foil (MTI, 18 µm) using a doctor blade coater and then dried at 60°C in a vacuum oven for 12 hours. AMBB electrodes were prepared by mixing LNMO (MTI), carbon black (Super P, MTI), LTMB-PEG400 (Sigma-Aldrich) at a mass ratio of 80/10/10 with methanol (Sigma-Aldrich) for 12 hours at 90°C. The ink was coated onto aluminum foil (MTI, 18 µm) with a doctor blade coater, and the *in-situ* polycondensation was carried out at 120°C in a vacuum oven for 12 hours. After coating, AMFB and AMBB electrodes were calendared in a hot rolling press at 80°C.

The electrodes underwent evaluation using an ECC-std EL-CELL® two-electrode and CR2032 Coin Cell test cell. Lithium foil is utilized as the anode, and 150 µL of 1 M LiPF<sub>6</sub> (EC:DMC:EMC 1:1:1 v/v) served as the electrolyte, impregnated on a 0.6 mm thick Whatman fiberglass spacer. The assembly of the electrochemical cells took place within an argon glove box, maintaining oxygen (O<sub>2</sub>) and water (H<sub>2</sub>O) concentration of less than 0.5 ppm. To conduct the electrochemical characterization, the cells were analyzed using a VMP-3 multichannel potentiostat.

### Samples characterization

The SLICPB was characterized by <sup>7</sup>Li and <sup>11</sup>B ss-NMR spectroscopy at room temperature under magic angle spin (MAS) conditions at 3.5 and 8 kHz on a Bruker AVANCE-II 300 NMR spectrometer, and with a Spectrum Two Perkin Elmer FTIR spectrometer. The DEMS evaluation of the electrode materials involved setting up an ECC-DEMS EL-CELL®. A porous PTFE membrane with a thickness of 60 µm and pores measuring 0.1 µm, with 50% porosity was interlinked between the cell and the 1/16" tubing with a valve and it was connected to a Teflon adapter in the DEMS equipment. The analysis was connected to the quadrupole mass spectrometer Prisma QMG220 to detect the formation of volatile species, particularly at oxidation potentials near 5 V through an Autolab potentiostat. The experiment comprised performing linear voltammetry to oxidize the material (battery charge) followed by chronoamperometry at a voltage of 5 V, while monitoring various volatile compounds such as hydrogen (2 m/z), carbon dioxide (44 m/z), ethylene or carbon monoxide (28 m/z), and oxygen (32 m/z).

To assess the impact of SLICPB on the structural stability of the material, EPR was conducted, as previous studies have demonstrated its effectiveness in determining the quantity of paramagnetic Mn<sup>2+</sup> ions.<sup>[59]</sup> The goal was to evaluate the formation of Mn<sup>2+</sup> ions, in the separator and the cathode. EPR spectra were recorded using a Bruker Elexsys E-500-II EPR spectrometer operating at X-band frequency (9.4315 GHz), equipped with 100 kHz field modulation and phase-sensitive detection to obtain the first derivative signal. The EPR measurements were performed at temperatures of 300 K. For signal intensity determination, peak-to-peak intensities were utilized, which were then verified using the double integration method for calibration. All continuous-wave EPR data were acquired under unsaturated slow passage conditions.

### Acknowledgements

This work was supported by Consejo Nacional de Ciencia y Tecnología (CONACYT) through Projects FORDECYT/1717328/2020, FORDECYT/1560240/2020, Ciencia Básica A1-S-15770 and IPN multidisciplinary project SIP-2181. The authors thank Dr. Miguel Angel Martinez-Cruz at Universidad Autónoma Metropolitana for helping with the ss-NMR spectra analysis and Dr. Miguel Angel Oliver-Tolentino for helping with the preliminary EPR measurements. The authors thank the project INFR-2011-1-163234, for the realization of the ss-NMR spectra. J.O.-G. acknowledges to CONACYT for the scholarship. R.G.G.H. thanks to L'oreal Foundation, UNESCO and Academia Mexicana de Ciencias. G.G.-G. thanks Ciencia de frontera rafCF-2023-I-253, A.M.-R. thanks SIP-IPN project 20231003 and D.R.R. is grateful to CONACYT (Project 225115) for EPR spectrometer acquisition.

### Conflict of Interests

The authors declare no conflict of interest.

### Data Availability Statement

The data that support the findings of this study are available from the corresponding author upon reasonable request.

**Keywords:** enhanced stability · in situ polymerization · lithium-ion batteries · LNMO cathode · single lithium-ion conducting polymer

- [1] M. Erakca, M. Baumann, W. Bauer, L. de Biasi, J. Hofmann, B. Bold, M. Weil, *iScience* **2021**, *24*, 102437.
- [2] D. L. Wood, J. Li, S. J. An, *Joule* **2019**, *3*, 2884–2888.
- [3] K. I. Ozoemena, M. Kebede, in *Nanostructure Sci. Technol. Nanomater. Adv. Batter. Supercapacitors* (Eds.: K. I. Ozoemena, S. Chen), Springer Nature, Switzerland, **2016**, p. 567.
- [4] K. Amine, H. Tukamoto, H. Yasuda, Y. Fujita, *J. Electrochem. Soc.* **1996**, *143*, 1607–1613.
- [5] L. D. Ellis, J. P. Allen, L. M. Thompson, J. E. Harlow, W. J. Stone, I. G. Hill, J. R. Dahn, *J. Electrochem. Soc.* **2017**, *164*, A3518–A3528.
- [6] B. Rowden, N. Garcia-Araez, *Energy Reports* **2020**, *6*, 10–18.
- [7] J. Lopez, D. G. Mackanic, Y. Cui, Z. Bao, *Nat. Rev. Mater.* **2019**, *4*, 312–330.
- [8] H. Xu, H. Zhang, J. Ma, G. Xu, T. Dong, J. Chen, G. Cui, *ACS Energy Lett.* **2019**, *4*, 2871–2886.
- [9] R. Benedek, *J. Phys. Chem. C* **2017**, *121*, 22049–22053.
- [10] B. Aktekin, M. Valvo, R. I. Smith, M. H. Sørby, F. Lodi Marzano, W. Zipprich, D. Brandell, K. Edström, W. R. Brant, *ACS Appl. Energ. Mater.* **2019**, *2*, 3323–3335.
- [11] Y. Han, Y. S. Jiang, F. Da Yu, L. Deng, W. Ke, S. J. Zhang, L. F. Que, B. Wu, F. Ding, L. Zhao, Z. B. Wang, *Adv. Funct. Mater.* **2022**, *32*, DOI 10.1002/adfm.202207285.
- [12] R. Qiao, Y. Wang, P. Olalde-velasco, H. Li, Y. Hu, W. Yang, *J. Power Sources* **2015**, *273*, 1120–1126.
- [13] N. P. W. Pieczonka, L. Yang, M. P. Balogh, B. R. Powell, K. Chemelewski, A. Manthiram, S. A. Krachkovskiy, G. R. Goward, M. Liu, J. H. Kim, *J. Phys. Chem. C* **2013**, *117*, 22603–22612.
- [14] L. Yang, T. Markmaitee, B. L. Lucht, *J. Power Sources* **2011**, *196*, 2251–2254.
- [15] J. Xia, L. Ma, J. R. Dahn, *J. Power Sources* **2015**, *287*, 377–385.
- [16] Y. Q. Chen, T. Y. Chen, W. D. Hsu, T. Y. Pan, L. J. Her, W. M. Chang, M. Wohlfahrt-Mehrens, H. Yoshitake, C. C. Chang, *J. Power Sources* **2020**, *477*, 228473.
- [17] L. Porcarelli, A. S. Shaplov, F. Bella, J. R. Nair, D. Mecerreyes, C. Gerbaldi, *ACS Energy Lett.* **2016**, *1*, 678–682.
- [18] S. K. Cho, K. S. Oh, J. C. Shin, J. E. Lee, K. M. Lee, J. Cho, W. B. Lee, S. K. Kwak, M. Lee, S. Y. Lee, *Adv. Funct. Mater.* **2022**, *32*, DOI 10.1002/adfm.202107753.
- [19] G. Guzmán-González, G. Ramos-Sánchez, L. E. Camacho-Forero, I. González, *J. Phys. Chem. C* **2019**, *123*, 17686–17694.
- [20] G. Guzmán-González, H. J. Avila-Paredes, I. Santos-Mendoza, *J. Solid State Electrochem.* **2023**, *27*, 2905–2915DOI 10.1007/s10008-023-05563-1.
- [21] K. Kikuchi, S. Tsuchitani, in *Ionic Conductive Polymers BT - Soft Actuators: Materials, Modeling, Applications, and Future Perspectives* (Eds.: K. Asaka, H. Okuzaki), Springer Japan, Tokyo, **2014**, pp. 81–93.
- [22] C. Wang, Y. Ma, G. Xu, G. Cui, *Batter. Energy* **2022**, *1*, 20220010.
- [23] R. Suárez-Hernández, G. Ramos-Sánchez, I. O. Santos-Mendoza, G. Guzmán-González, I. González, *J. Electrochem. Soc.* **2020**, *167*, 100529.
- [24] R. Del Olmo, G. Guzmán-González, I. O. Santos-Mendoza, D. Mecerreyes, M. Forsyth, N. Casado, *Batter. Supercaps* **2023**, *6*, e202200519 DOI 10.1002/batt.202200519.
- [25] H. J. Song, S. H. Jang, J. Ahn, S. H. Oh, T. Yim, *J. Power Sources* **2019**, *416*, 1–8.
- [26] Y. Wang, Y. Zhang, S. Wang, S. Dong, C. Dang, W. Hu, D. Y. W. Yu, *Adv. Funct. Mater.* **2021**, *31*, 1–10.
- [27] S. Wu, Y. Yang, C. Liu, T. Liu, Y. Zhang, B. Zhang, D. Luo, F. Pan, Z. Lin, *ACS Energy Lett.* **2021**, *6*, 290–297.
- [28] Y. Liu, R. Zhang, J. Wang, Y. Wang, *iScience* **2021**, *24*, 102332.
- [29] C. Yuan, Y. Deng, T. Li, F. Yang, *CIRP Ann. - Manuf. Technol.* **2017**, *66*, 53–56.
- [30] K. W. Knehr, T. Hodson, C. Bommier, G. Davies, A. Kim, D. A. Steingart, *Joule* **2018**, *2*, 1146–1159.
- [31] G. Guzmán-González, H. J. Ávila-Paredes, E. Rivera, I. González, *ACS Appl. Mater. Interfaces* **2018**, *10*, 30247–30256.
- [32] J. Ma, Z. Wang, J. Wu, Z. Gu, X. Xin, X. Yao, *Batteries* **2023**, *9*, 28DOI 10.3390/batteries9010028.
- [33] M. Zhu, J. Ma, Z. Wang, H. He, X. Yao, *J. Power Sources* **2023**, *585*, 233651.
- [34] X. Li, M. Tang, X. Feng, I. Hung, A. Rose, P. H. Chien, Z. Gan, Y. Y. Hu, *Chem. Mater.* **2017**, *29*, 8282–8291.
- [35] A. Maurel, M. Armand, S. Gruegeon, B. Fleutot, C. Davoisne, H. Tortajada, M. County, S. Panier, L. Dupont, *J. Electrochem. Soc.* **2020**, *167*, 70536.
- [36] Q. Ma, X. Qi, B. Tong, Y. Zheng, W. Feng, J. Nie, Y.-S. Hu, H. Li, X. Huang, L. Chen, Z. Zhou, *ACS Appl. Mater. Interfaces* **2016**, *8*, 29705–29712.
- [37] J. L. Olmedo-Martínez, M. Pastorío, E. Gabirondo, A. Lorenzetti, H. Sardon, D. Mecerreyes, A. J. Müller, *Polymers (Basel)*. **2021**, *13*, DOI 10.3390/polym1312097.
- [38] Z. Wang, L. Shen, S. Deng, P. Cui, X. Yao, *Adv. Mater.* **2021**, *33*, 2100353.
- [39] Q. Ma, H. Zhang, C. Zhou, L. Zheng, P. Cheng, J. Nie, W. Feng, Y. S. Hu, H. Li, X. Huang, L. Chen, M. Armand, Z. Zhou, *Angew. Chem. Int. Ed.* **2016**, *55*, 2521–2525.
- [40] Y. Chen, W. Huo, M. Lin, L. Zhao, *PLoS One* **2018**, *13*, e0189757.
- [41] A. Oishi, R. Tatara, E. Togo, H. Inoue, S. Yasuno, S. Komaba, *ACS Appl. Mater. Interfaces* **2022**, *14*, 51808–51818.
- [42] Y. Kwon, Y. Lee, S. O. Kim, H. S. Kim, K. J. Kim, D. Byun, W. Choi, *ACS Appl. Mater. Interfaces* **2018**, *10*, 29457–29466.
- [43] K. E. Madsen, K. A. Wade, R. T. Haasch, D. B. Buchholz, K. L. Bassett, B. G. Nicolau, A. A. Gewirth, *ACS Appl. Mater. Interfaces* **2019**, *11*, 39890–39901.
- [44] L. Wu, H. Huo, Q. Zhou, X. Yin, Y. Ma, J. Wang, C. Du, P. Zuo, G. Yin, Y. Gao, *ACS Appl. Energy Mater.* **2022**, *5*, 6401–6409DOI 10.1021/acsaem.2c00837.
- [45] Z. Jusys, M. Binder, J. Schnaidt, R. J. Behm, *Electrochim. Acta* **2019**, *314*, 188–201.
- [46] Z. Liu, P. Hu, J. Ma, B. Qin, Z. Zhang, C. Mou, Y. Yao, G. Cui, *Electrochim. Acta* **2017**, *236*, 221–227.
- [47] S. Hein, T. Danner, D. Westhoff, B. Prifling, R. Scurtu, L. Kremer, A. Hoffmann, A. Hilger, M. Osenberg, I. Manke, M. Wohlfahrt-Mehrens, V. Schmidt, A. Latz, *J. Electrochem. Soc.* **2020**, *167*, 013546.
- [48] V. A. Nguyen, C. Kuss, *J. Electrochem. Soc.* **2020**, *167*, 065501.
- [49] N. Vicente, M. Haro, D. Cíntora-Juárez, C. Pérez-Vicente, J. L. Tirado, S. Ahmad, G. García-Belmonte, *Electrochim. Acta* **2015**, *163*, 323–329.
- [50] W. Choi, H.-C. Shin, J. M. Kim, J.-Y. Choi, W.-S. Yoon, *J. Electrochem. Sci. Technol* **2020**, *11*, 1–13.
- [51] J. Bisquert, G. García-Belmonte, P. Bueno, E. Longo, L. O. S. Bulhões, *J. Electroanal. Chem.* **1998**, *452*, 229–234.
- [52] A. M. Tripathi, W.-N. Su, B. J. Hwang, *Chem. Soc. Rev.* **2018**, *47*, 736–851.
- [53] B. Michalak, B. B. Berkes, H. Sommer, T. Bergfeldt, T. Brezesinski, J. Janek, *Anal. Chem.* **2016**, *88*, 2877–2883.
- [54] B. B. Berkes, A. Jozwiuk, M. Vrácár, H. Sommer, T. Brezesinski, J. Janek, *Anal. Chem.* **2015**, *87*, 5878–5883.
- [55] B. L. D. Rinkel, D. S. Hall, I. Temprano, C. P. Grey, *J. Am. Chem. Soc.* **2020**, *142*, 15058–15074.
- [56] J. N. Zhang, Q. Li, Y. Wang, J. Zheng, X. Yu, H. Li, *Energy Storage Mater.* **2018**, *14*, 1–7.
- [57] P. Mu, H. Zhang, H. Jiang, T. Dong, S. Zhang, C. Wang, J. Li, Y. Ma, S. Dong, G. Cui, *J. Am. Chem. Soc.* **2021**, *143*, 18041–18051.
- [58] H. Nguyen, R. J. Clément, *ACS Energy Lett.* **2020**, *5*, 3848–3859.
- [59] J. C. Hestenes, J. T. Sadowski, R. May, L. E. Marbella, *ACS Mater. Au* **2022**, *3*, 88–101, DOI 10.1021/acsmaterialsau.2c00060.
- [60] M. Jiang, P. Mu, H. Zhang, T. Dong, B. Tang, *Nano-Micro Lett.* **2022**, *14*, 87.

Manuscript received: September 7, 2023

Revised manuscript received: November 8, 2023

Accepted manuscript online: November 17, 2023

Version of record online: December 5, 2023